β-alumina-14*H* and β-alumina-21*R*: Two chromic $Na_{2-\delta}(Al,Mg,Cr)_{17}O_{25}$ polysomes observed in slags from the production of low-carbon ferrochromium

Clivia Hejny[a,], Volker Kahlenberg[a], Daniela Schmidmair[a], Martina Tribus[a], Johan deVilliers[b]

[a] Institute of Mineralogy and Petrography, University of Innsbruck, Innrain 52, A-6020 Innsbruck, Austria

[b] Department of Materials Science and Metallurgical Engineering, University of Pretoria, Mineral Science Building, SouthAfrica

Graphical abstract

Two new phases related to the structures of β- and β´´-alumina with a composition of $Na_{2-\delta}(Al, Mg, Cr)_{17}O_{25}$ were found to be composed of an alternating stacking of a spinel-type and a Na-hosting block. In contrast to the structures of hitherto known β-aluminas the spinel-type block in $N_{2-\delta}(Al, Mg, Cr)_{17}O_{25}$ is composed of five cation layers rather than three cation layers.

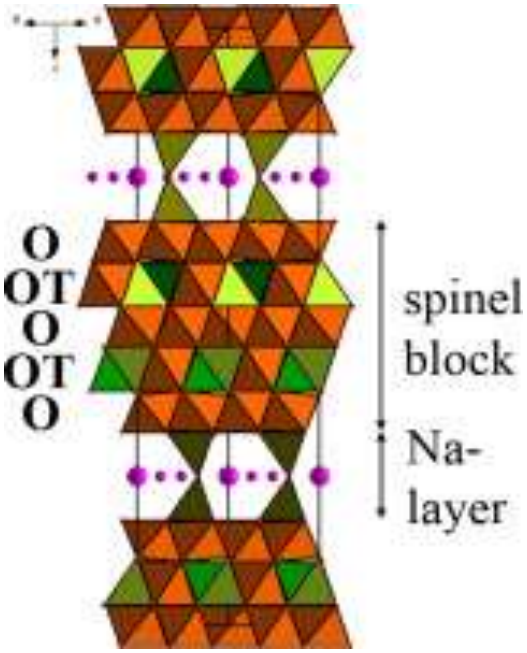

Abstract

The crystal structures of unknown phases found in slags from the production of low-carbon ferrochromium were studied by powder and single-crystal X-ray diffraction. Two phases of $Na_{2-\delta}(Al, Mg, Cr)_{17}O_{25}$ composition were found to be composed of an alternating stacking of a spinel-type and a Na-hosting block. Similar structures are known for β-alumina and β”-alumina, $NaAl_{11}O_{17}$. However, the spinel-type block in $Na_{2-\delta}(Al, Mg, Cr)_{17}O_{25}$ is composed of five cation layers in contrast to three cation layers in the β-alumina spinel-block. The two new phases, β-alumina-14*H*, *P63/mmc*, a=5.6467(2), *c*=31.9111(12) Å, and β-alumina-21*R*,

R $\bar{3}$*m*, *a*=5.6515(3), *c*=48.068(3) Å have a 14-layer and 21-layer stacking with a 2 × (*ccccccch*) and a 3 × (*cccccccc*) repeat sequence of oxygen layers in cubic and hexagonal close packing, respectively.

Keywords

β-alumina; Polysome; Crystal structure

1. Introduction

In the production of stainless steel from ferrochrome and scrap metal, extensive decarburization is necessary to reduce the carbon content to very small amounts (<0.04%) in stainless and low carbon steels. Since the introduction of the argon-oxygen decarburization (AOD) and vacuum-oxygen decarburization (VOD) processes the principal chromium source is high-carbon ferrochrome [7].

The presence of higher amounts of carbon creates problems in special low carbon alloy steels, often referred to as sensitisation caused by the formation of chromium carbide $Cr_{23}C_6$. This leads to loss of corrosion resistance, which is the prime function of these steels. Extra-low carbon ferrochromium containing 0.02–0.05% carbon is considered one of the ferroalloys necessary for the production of some high quality steel grades, especially the corrosion- resistant and high-temperature oxidation-resistant steels [14].

Because of the complications described above the aluminothermic reduction of chromite has been investigated to produce extra-low carbon ferrochrome to be used as an additive to special steels. Since the product of the reduction is alumina with a very high melting point, fluxing agents such as sodium salts are added to produce a liquid slag that can be tapped and to facilitate alloy separation [7].

A series of experiments were done to test the feasibility of producing low carbon ferrochrome from chromite using aluminothermic reduction. The tests were designed based on chemical assays of the chromite, aluminium and flux raw materials, and thermochemical calculations. The chromite contained approximately 51 mass % Cr_2O_3 and had a Cr:Fe ratio of 2.25. The aluminium had a purity of 99.5% and the fluxes ($NaNO_3$ and $NaClO_3$) had purities of more than 97%.

The mixture of raw materials was ignited and left to react autogenously, heated by the exothermic reduction reaction. Calculated adiabatic temperatures were in excess of 1800 °C. Heat losses caused the actual temperatures to be lower, but these were not measured. The products were left to cool in air and the metal and slag were separated once it achieved a temperature that allowed handling.

Examination of the slag revealed the presence of unknown phases that are not present either in the ICSD or in the ICDD databases [3] and [15]. They seemed to be related to the β-alumina phases but they contain substantial amounts of chromium. It was therefore deemed necessary to investigate these phases crystallographically in order to characterise them with the aim of identification and also for quantification by X-ray powder diffraction using the Rietveld method.

On the other hand, the β-alumina family of materials is a group of Na-aluminates of technical importance in aluminium production and as fast ionic conductors. The latter have been considered as candidates to substitute for lithium batteries for a long time [18]. Although β-alumina was discovered a hundred years ago in 1916, and has been studied intensively in the 1970s and 1980s (see [25] and references cited therein) the exact mechanism of ionic conductivity in the β-aluminas is still not fully understood and is the focus of attention [27].

2. Experimental

2.1. Electron microprobe analysis

The piece of slag used for analysis had a bulky appearance of dark green to greenish black colour with coarsely crystalline matrix. In order to study its chemical composition microprobe analysis was performed with an electron microprobe (JEOL JXA 8100 SUPERPROBE) operated in wavelength-dispersive analytical mode with an acceleration voltage of 15 kV, 10 nA beam current and counting times of 20 s for the peak and 10 s for the lower and upper background. Natural and synthetic standards were used for calibration (Jadeite, MgO, rutile, chromite, corundum and rhodonite). The minerals were measured using a rastered beam with a raster size of 4×6 μm^2.

Backscattered electron images (Fig. 1) reveal the majority of the sample to be composed of phases with parallel cleavage that were later identified as Cr-bearing β-alumina related compounds. Additional grains of spinel and corundum appear in slightly brighter grey and droplets of chromium are intensive white. Additionally, minor quantities of titanium-oxide phases, an unidentified Al-Cr-Ti-oxide-phase and an unidentified Mg-Mn-Cr-phase where detected.

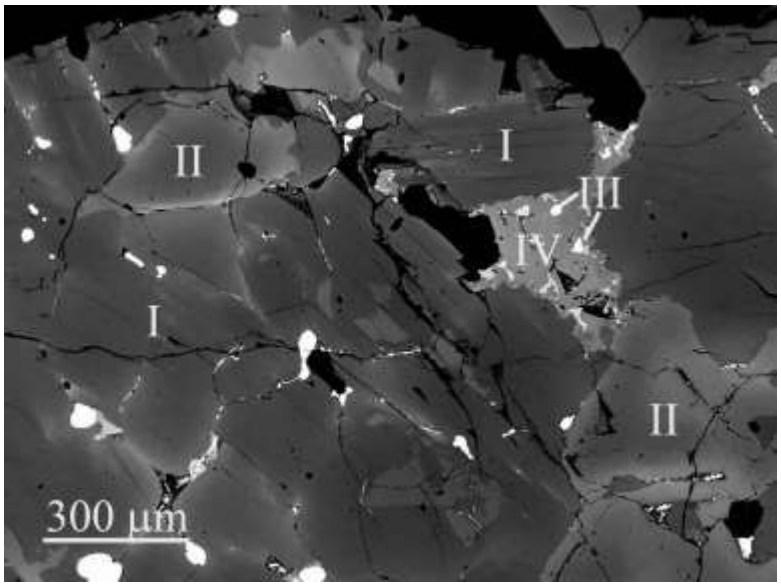

Fig. 1. Backscattered electron image of the slag showing the majority of the sample being composed of (I) Cr-bearing β-alumina-related phases with parallel cleavage, (II) spinel and corundum, with additions of (III) bright coloured droplets of chromium and (IV) minor quantities of unidentified oxide phases containing Ti, Al-Cr-Ti, and Mg-Mn-Cr.

Spinel was found to be zoned (Fig. 2) with an enrichment of chromium and traces of titanium and manganese on the cost of aluminium and magnesium contents towards the rim. The

average of twelve analysed spots on several spinel grains in the polished slag sample gave a formula of $(Mg, Mn)_{0.50}(Al, Cr, Ti)_{2.33}O_4$. In the core the Mn and Ti content was insignificant and towards the rim a maximum of 0.011 Mn and 0.015 Ti atoms per formula unit was detected. The derived formula is in consistency with non-stoichiometric spinels formed at temperatures above 1000 °C, that can accommodate a great degree of Al_2O_3 excess [19]. Furthermore, four spot analysis of an apparent spinel phase (as estimated by the contrast and appearance of the grains) showed them to be a Cr-corundum containing minor amounts of Ti with an average composition of $(Al_{1.689}Cr_{0.286}Ti_{0.016})_{\Sigma 1.991}O_3$.

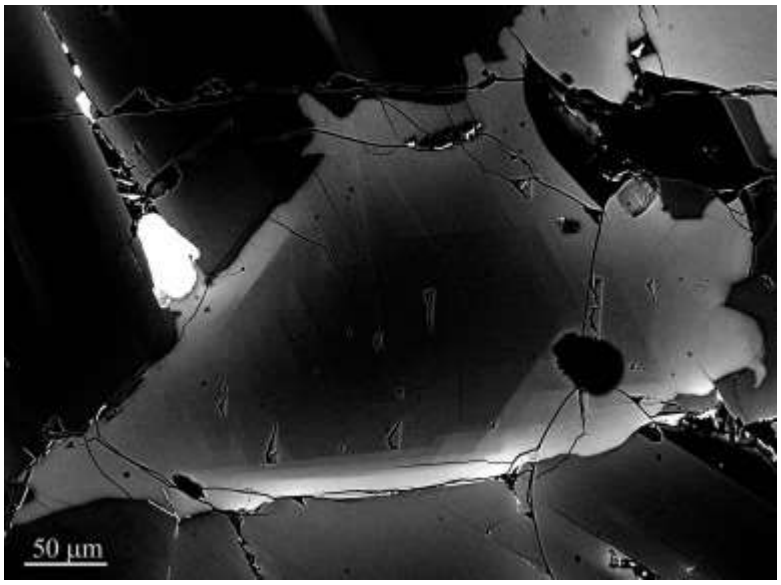

Fig. 2. Backscattered electron image of a zoned spinel grain in the slag. The core is enriched with aluminium and magnesium in comparison to the rim whereas traces of chromium, titanium and manganese increase towards the outer, brighter zones of the grain.

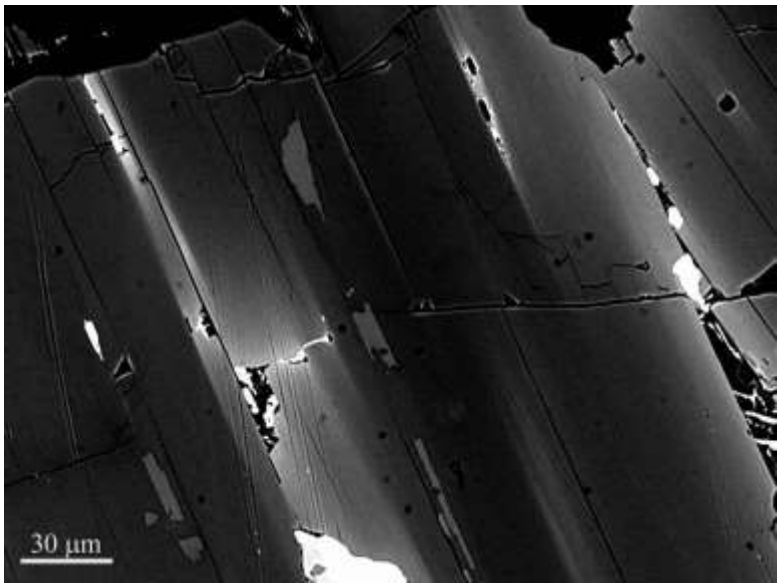

Fig. 3. Backscattered electron image of the Cr-bearing β-alumina related phases showing parallel cleavage. Striking variations in the contrast parallel to the cleavage indicates variations of the (Al+Mg)- versus Cr-content.

Similarly to the spinel phase the Cr-bearing β-alumina related phases with parallel cleavage (Fig. 3) show variations of the contrast that could be shown to be related to variation of the aluminium plus magnesium content in exchange for chromium. However, these changes in the contrast are apparently not correlated with the Na-content. The exact chemical analysis of the Cr-bearing β-alumina related compounds proved to be difficult, because the sample decomposed during analysis: The observation that the sum of the elemental analysis never reached 100% lead to the probable explanation that Na is lost under exposure of the electron

Table 1. Electron microprobe analyses of β-alumina-14*H* and β-alumina-21*R*; elements normalised on 25 oxygen atoms from eleven individual spot analyses.

	# 12	**# 15**	**# 18**	**# 19**	**# 20**	**# 21**	**# 22**	**# 23**	**# 31**	**# 32**	**# 34**	**Min**	**Max**
Na	1.68	0.86	0.54	0.59	1.50	1.86	1.61	0.89	1.43	1.68	1.22	0.54	1.86
Mg	1.79	1.83	1.64	1.61	1.70	1.54	1.84	1.48	1.89	1.65	1.66	1.48	1.89
Ti	0.04	0.01	0.02	0.02	0.02	0.05	0.01	0.13	0.01	0.02	0.02	0.01	0.13
Cr	1.00	0.60	1.11	1.04	0.93	1.29	0.56	1.60	0.53	1.17	0.99	0.53	1.60
Al	13.86	14.54	14.24	14.32	14.06	13.64	14.32	13.59	14.38	13.79	14.13	13.79	14.54
Mn	0.02	0.01	0.03	0.03	0.03	0.04	0.01	0.05	0.02	0.03	0.03	0.01	0.05
Σ cations	18.39	17.85	17.58	17.61	18.24	18.42	18.35	17.74	18.26	18.34	18.05		

beam. Several points of analysis (Table 1) normalised to 25 oxygen atoms as derived from structure analysis (see later) gave the following simplified formula: $Na_{2-\delta}(Al, Mg, Cr)_{17}O_{25}$.

Further to this chemical analysis performed on the polished slag sample it was also tried to derive a formula from selected single crystals, of which lattice parameters had been determined prior to the electron microprobe analysis and in one case also a full intensity data set had been collected. These single crystals were placed on a carbon tape for the chemical analysis. However, the results were even less reliable to a point that they could not be used to calculate a chemical formula and to compare it with the formula obtained from the refinement of the single crystal data. Imaging showed that some of the single crystals broke apart under the electron beam.

2.2. Single crystal X-ray diffraction

Several single crystal fragments of green colour were selected under polarised light for clarity and sharp extinction and checked for their lattice parameters. It was noticed, that two sets of lattice parameters were found: Many crystals had a hexagonal *P*-lattice with $a \approx 5.65$ Å, $c \approx 32.10$ Å, and some crystals had an *R*-centred trigonal lattice with $a \approx 5.65$ Å, $c \approx 48.07$ Å. In comparison to related spinel-, β-alumina-type-, magnetoplumbite- and högbomite-structures, [1], [5], [6], [16], [17] and [22], this lead to the suggestion, that the structures reported here

are likewise composed of close-packed oxygen layers with a thickness of ca. 2.3 Å. Crystals with c≈32.10 Å have a 14-layer (or 2×7-layer) repeat sequence and crystals with c≈48.07 Å

Table 2. Data collection and refinement parameters.

	β-alumina-21*R*	**β-alumina-14*H***
Crystal data		
Formula from refinement	Na1.923(Al, Mg)16.752Cr0.248O25	Na1.905(Al, Mg)16.726Cr0.274O25
Space group	R$\bar{3}$m (No. 166)	P63/mmc (No. 194)
a [Å]	5.6515(3)	5.6467(2)
c [Å]	48.068(3)	31.9111(12)
V [Å3]	1329.8(1)	881.17(6)
Z	3	2
V / Z	443.3	440.6
Density (calculated) [g/cm3]	3.491	3.4272
Absorption coefficient [mm−1]	1.697	1.264
Intensity measurements		
Crystal size [mm]	0.06×0.12×0.17	0.07×0.13×0.23
Diffractometer	Oxford Diffraction Gemini R Ultra	Oxford Diffraction Gemini R Ultra
Monochromator	Graphite	Graphite
Radiation type, source	X-ray, MoKα	X-ray, MoKα
Data collection temperature [°C]	21	21
Generator settings [kV, mA]	50, 40	50, 40
Detector, distance [mm]	CCD, 70	CCD, 70
Scan width [°]	0.5	0.5
Measurement time /frame [sec]	22.5	40

	β-alumina-21*R*	β-alumina-14*H*
Index ranges	−7≤ h ≤6	−7-≤ h ≤7
	−4≤ k ≤7	−5≤ k ≤7
	−58≤ l ≤61	−41≤ l ≤40
No. of reflections collected	2795	5343
No. of unique reflections	487	498
No. of observed reflections (I >3σ(I)	407	453
Absorption correction	9 faces	10 faces
R(int) after absorption correction	2.52	2.30
Refinement parameters		
No. of parameters	39	38
Final R indices [I>3sigma(I)]	R1=0.0442, wR2=0.0526	R1=0.0393, wR2=0.0627
Final R indices (all data)	R1=0.0540, wR2=0.0544	R1=0.0424, wR2=0.0631
Goodness-of-fit on F	0.0222	0.0427
Largest diff. peak and hole [e/Å3]	0.67 and −0.61	0.85 and −1.13

have a 21-layer (or 3×7-layer) repeat sequence. In analogy to the nomenclature suggested for different members of the högbomite polysomatic series[1][2] the two different β-alumina related structures will be referred to as β-alumina-14*H* and β-alumina-21*R*. In this nomenclature the suffixes n*R* and n*H* stand for n oxygen layers of ca. 2.3 Å thickness and *R* and *H* for rhombohedral (trigonal) or hexagonal symmetry, respectively. Selected crystals of both phases were subsequently mounted for single-crystal X-ray diffraction full-intensity data collection on an Oxford Diffraction Gemini four-circle diffractometer, equipped with a Ruby CCD detector and using graphite-monochromatized Mo-*K*α radiation (50 kV, 40 mA). Data collection was performed at room temperature. Data reduction included intensity integration, background and Lorentz-polarisation correction performed with the *CrysAlisPRO* software package [24]. The morphologies of the crystal fragments were approximated by external faces and an analytical absorption correction based on these indexed faces was applied. The structures were solved by charge flipping with the program *SUPERFLIP* [20] and refined with the program *JANA2006* [23]. Experimental details of data collection and structure refinement are summarised in Table 2, atomic coordinates, interatomic distances and bond valences [11] of the refined structures are given in Table 3, Table 4 and Table 5. Both crystal

structure refinements were performed with scattering factors for neutral atoms with isotropic displacement parameters for all atoms apart from Na. In the initial stages of the structure refinement Al and Mg were - due to their similar scattering contribution - both refined together as Al on all sites and Cr was initially placed together with Al/Mg on the octahedral sites. The Cr substitution for Al was subsequently refined, the resulting optimized cation assignment is given in Table 4 and Table 5 for β-alumina-14*H* and β-alumina-21*R*, respectively, and will be discussed later.

Table 3. Atomic coordinates.

		β-alumina-21R	β-alumina-14H
M1	x	0.66667	0.333333
	y	0.33333	0.666667
	z	0.11869(4)	0.07229(5)
	Uiso	0.0055(7)	0.0057(6)
M2	x	0.33333	0.5
	y	0.16667	0
	z	0.16667	0
	Uiso	0.0076(5)	0.0083(4)
M3	x	0.49827(11)	0.16493(8)
	y	0.50173(11)	0.32985(16)
	z	0.06829(3)	0.14842(3)
	Uiso	0.0058(4)	0.0056(4)
T4	x	0	0.666667
	y	0	1.333333
	z	0.10578(4)	0.09106(7)
	Uiso	0.0067(5)	0.0081(5)
T5	x	0.33333	0
	y	0.66667	0

	z	0.20357(5)	0.05568(5)
	Uiso	0.0100(5)	0.0112(5)
T6	x	0	0.666667
	y	0	0.333333
	z	0.03522(4)	0.19770(5)
	Uiso	0.0072(5)	0.0088(5)
Na1	x	0.6069(13)	0
	y	0.3931(13)	0
	z	−0.0015(2)	0.25
	Ueq	0.111(6)	0.171(5)
Na2	x		0.5274
	y		0.7637
	z		0.25
	Ueq		0.163(15)
O1	x	0.33333	0.333333
	y	0.66667	0.666667
	z	0.24275(10)	0.17414(12)
	Uiso	0.0096(11)	0.0090(9)
O2	x	0.66667	0.3302(4)
	y	0.33333	0.16512(18)
	z	0.05095(9)	0.17726(7)
	Uiso	0.0071(11)	0.0100(6)
O3	x	0.1677(2)	0
	y	0.3354(5)	0

	z	**0.04930(6)**	0.11523(12)
	Uiso	**0.0089(7)**	0.0112(9)
O4	x	0.1520(3)	0.0226(4)
	y	0.3040(5)	0.5113(2)
	z	0.18946(6)	0.10811(8)
	Uiso	0.0080(7)	0.0115(6)
O5	x	0.3573(5)	0.666667
	y	0.1787(3)	0.333333
	z	0.09491(6)	0.03422(13)
	Uiso	0.0094(7)	0.0110(9)
O6	x	0	0.1807(2)
	y	0	0.8193(2)
	z	0.14432(10)	0.03444(8)
	Uiso	0.0066(10)	0.0116(6)
O7	x	0.045(3)	0.6667
	y	0.045(3)	0.3333
	z	0	0.25
	Uiso	0.008(4)	0.057(3)

Table 4. Interatomic distances [Å] in β-alumina-21*R* [Å].

				Occupancy	bvs [v.u.]
M1-O4	OT	(3×)	1.918(3)	0.96(1) Al/Mg: 0.04(1) Cr	2.80(1)
M1-O5		(3×)	1.897(3)		
M2-O4	O (central)	(4×)	1.910(3)	1.0 Al/Mg	2.64(1)
M2-O6		(2×)	1.953(3)		
M3-O1	O (rim)	(1×)	1.938(3)	0.97(1) Al/Mg: 0.03(1) Cr	2.69(1)
M3-O2		(1×)	1.847(2)		
M3-O3		(2×)	1.858(3)		
M3-O		(2×)	2.037(3)		
T4-O5	OT	(3×)	1.825(3)	1.0 Mg/Al	2.26(1)
T4-O6		(1×)	1.853(5)		
T5-O1	OT	(1×)	1.884(5)	1.0 Mg/Al	1.90(1)
T5-O4		(3×)	1.900(3)		
T6-O3	Na-block	(3×)	1.776(3)	1.0 Al/Mg	2.75(1)
T6-O7		(1×)	1.712(3)		
Na-O2	Na-block	(1×)	2.589(11)	3×0.32(1) Na	
Na-O3		(3×)	2.701(9)		
Na-O7		**(3×)**	2.78(2)–3.25(2)		

Table 5. Interatomic distances [Å] in β-alumina-14*H*.

				Occupancy	bvs [v.u.]
M1-O4	OT	(3×)	1.901(2)	0.94(1) Al/Mg: 0.06(1) Cr	2.79(1)
M1-O6		(3×)	1.920(2)		
M2-O5	O (central)	(2×)	1.962(2)	1.0 Al/Mg	2.61(1)
M2-O6		(4×)	1.913(2)		
M3-O1	O (rim)	(1×)	1.840(2)	0.97(1) Al/Mg: 0.03(1) Cr	2.70(1)
M3-O2		(2×)	1.858(2)		
M3-O3		(1×)	1.930(2)		
M3-O4					
(2×)	2.043(2)				
T4-O4	OT	(4×)	1.820(2)	1.0 Mg/Al	2.32(1)
T4-O5		(1×)	1.826(5)		
T5-O3	OT	(1×)	1.900(4)	1.0 Mg/Al	1.90(1)
T5-O6		(3×)	1.893(2)		
T6-O2	Na-block	(3×)	1.770(2)	1.0 Al/Mg	2.88(1)
T6-O7		(1×)	1.669(2)		
Na1-O2	Na-block	(6×)	2.828(2)	1.0 Na	
Na1-O3		(3×)	3.2601(3)		
Na2-O1	Na-block	(2×)	2.600(4)	3×0.30(1) Na	
Na2-O2		(4×)	3.099(2)		
Na2-O7		(2×)	2.9044(3)		

In the later stages of the refinement of β-alumina-21*R* a difference Fourier synthesis showed three maxima around the Na-position. Therefore, the Na position and its occupancy were refined as a split position. Likewise, O7 was refined as a split position, which reduced the R1- value from 0.061 to 0.044 and U_{ISO} of O7 to a value comparable to the U_{ISO} values of the other oxygen atoms in the structure refinement. A remaining positive maximum on the 3-fold

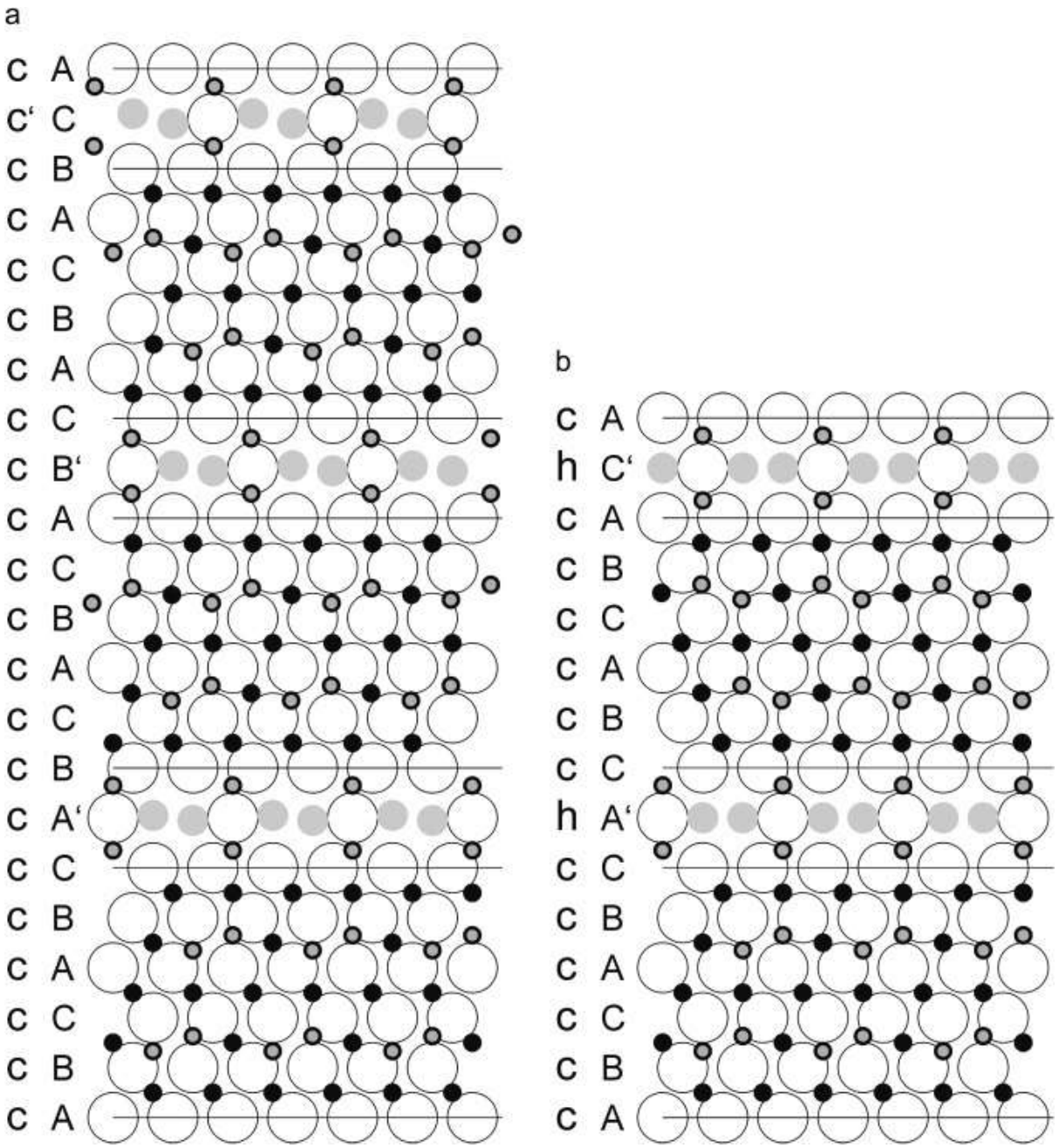

Fig. 4. Stacking of close packed oxygen layers in (a) β-alumina-21*R* and (b) β-alumina-14*H*. Large empty circles are for oxygen atoms, smaller grey filled circles for Na atoms, small black filled circles for octahedral positions, small grey circles with black rim for tetrahedral positions.

axis in the middle of the split Na-position was interpreted as truncation effect of the Fourier synthesis and could be eliminated by an anisotropic refinement of Na. The temperature parameters of all other atoms were kept isotropic, because the use of anisotropic displacement parameters for all atoms would overstress the ratio of observed reflection (measured up to d=0.74 Å) to parameters. In β-alumina-14*H* two different Na positions have been found, one with full occupation, Na1, and an additional split position that is not fully occupied, Na2.

2.3. Powder X-ray diffraction and phase quantification

Powder X-ray diffraction profiles were collected with a Bruker D8-Discover diffractometer in Bragg-Brentano θ−2θ geometry using Cu Kα1 radiation (40 kV, 40 mA) from 3 to 135°2θ with a counting time of 1 s per step and a step size of 0.01°2θ. The diffractometer is equipped with a primary beam Ge-monochromator. Primary and secondary Soller slits were used and a fixed divergence slit was set to an opening angle of 0.3°. Diffraction data were collected with a LYNXEYE™ silicon strip detector. Rietveld analysis was performed on the sample using the TOPAS Version 4.2 software [12], whereby peak profiles were calculated by the fundamental parameter approach [13]. For simulation of the background Chebychev polynomials of the 6th order were applied. During refinement lattice parameters and peak widths of four phases, i.e. β-alumina-14*H*, β-alumina-21*R*, spinel and chromium, were fitted, as well as the Al versus Cr occupancy on the octahedral positions of the two *b*-alumina polysomes. Preferred orientation of the (001) and (110) plane was accounted for with the March-Dollase function. The refinement converged to final R-values of 0.0637 for Rp, 0.0917 for Rwp and 0.0271 for GOF.

2.3.1. Description of the crystal structures

The structures of β-alumina-14*H* and β-alumina-21*R* are composed of close packed oxygen layers with a defect oxygen layer in every seventh sheet (Fig. 4(a),(b)). Within a seven-layer block six layers of cubic stacking type can be described as a spinel block with Al, Cr and Mg

situated on octahedral and tetrahedral voids. The cation sheets in the spinel block are composed of three layers with octahedrally coordinated cations (M) labelled **O**-layers (Fig. 5(a)) and two layers of tetrahedrally (T) and octahedrally coordinated cations labelled **OT**-layer (Fig. 5(b)). The **O**-layer has a composition of M_3O_4, the **OT**-layer has a composition of T_2MO_4. The spinel block has an **O**-**OT**-**O**-**OT**-**O** layer arrangement, thus the composition of the complete spinel block is $3\times M_3O_4+2\times T_2MO_4=T_4M_{11}O_{20}$. In the defect seventh oxygen sheet three out of four oxygen atoms per unit cell are replaced by a varying amount of sodium ions (Fig. 6(a)). Above and below of this defect Na-hosting oxygen layer Al is situated in tetrahedral voids. In case of full occupancy of the Na-sites this Na-block has a composition of $Na_2T_2O_5$, so that the overall formula of β-alumina-*14H* and −21*R* is $Na_2T_6M_{11}O_{25}$, which can

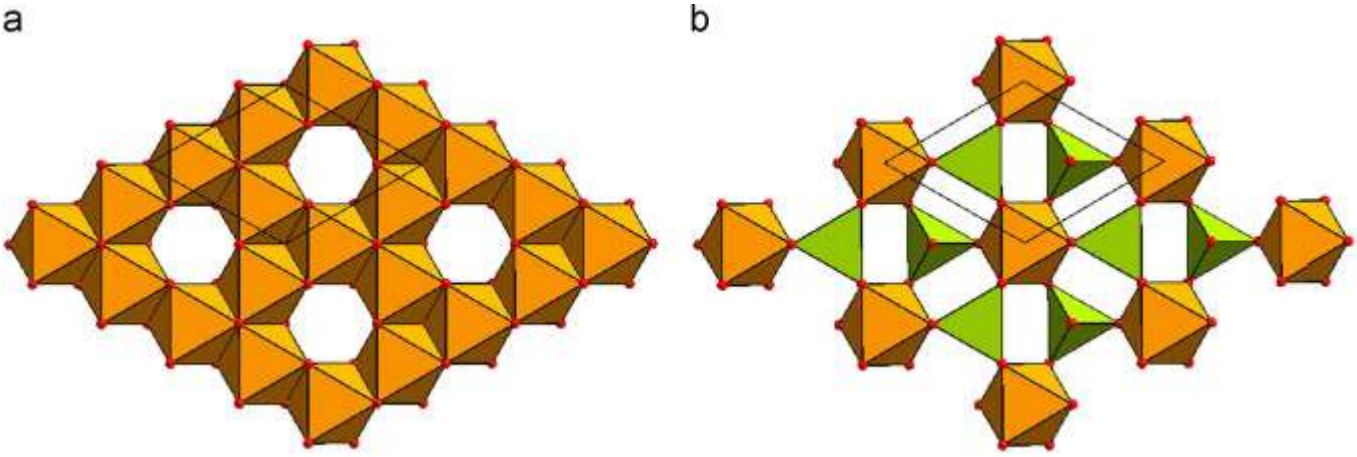

Fig. 5. (a) Polyhedral model of the **O**-layer (composition M_3O_4) and (b) **OT**-layer (composition T_2MO_4) of the spinel block.

be simplified as $Na_2{\times}_{17}O_{25}$, or including the fact that the two principle Na-sites are not fully occupied $Na_{2-\delta}{\times}_{17}O_{25}$. For reasons of charge balance it is not possible to have all tetrahedral and octahedral positions fully occupied by Al only. However, considering (1) that also Mg was found with electron microprobe analysis and (2) comparing the charge balance compensation mechanism for excess Na ions via Mg replacing Al in the β-alumina-type phases the following simplified composition can be given for β-alumina-14*H* and β-alumina-21*R*: $Na_{2-\delta}(Al, Cr, Mg)_{17}O_{25}$. The Na-block is comparable to the so-called conduction plane of the β-alumina-type family. It differs in β-alumina-14*H* and β-alumina-21*R* in a similar way as β-alumina and β”-alumina have different conduction planes.

The difference between β-alumina-14*H* and β-alumina-21*R* can be explained by the different stacking sequences of the oxygen layers and the resulting differences in the conduction layer as well as overall repeat sequence of the whole spinel-block and conduction layer arrangement: In β-alumina-21*R* all oxygen layers are in cubic close packing and three seven-layers units, each composed of a spinel block and a Na-block, are stacked according to an *R*-centring to give a repeat sequence of 21 layers (Fig. 4(a) and Fig. 7). The sequence of oxygen layers is …(ABCABC)A’(BCABCA)B’(CABCAB)C’… (Table 6), where the spinel layers are in parentheses and the defect oxygen layer is marked with an apostrophe, indicating that the oxygen atom in this defect layer is also in the position of close packing, i.e. in the position of cubic close packing in β-alumina-21*R*. In β-alumina-14*H* (Fig. 4(b) and Fig. 8) the oxygen layers of the spinel block are likewise in cubic close packing, “*c*”. However, the defect oxygen layer hosts a mirror plane and is adjacent by two oxygen layers in the same relative position and hence in a hexagonal close-packed environment, “*h*”. Two seven-layer units, each composed of one spinel and one Na-block, repeat per unit cell with an oxygen layer sequence of …(ABCABC)A’(CBACBA)C’…, or in an alternative description 2 × (*cccccch*).

Due to this different geometry of the Na-block, Na has a different coordination in β-alumina-14*H* and β-alumina-21*R*. In Fig. 6 the situation is explained for an ideal case with Na (green filled circles) being placed on the three-fold axis: Fig. 6(a) shows the central deficient oxygen layer of the Na-block with the two possible sites for Na. In Fig. 6(b) the oxygen-deficient Na-hosting layer is sandwiched between two adjacent oxygen layers in the same relative position (circles with grey filling), i.e. in hexagonal close packing (“ABA”-type) as found in β-alumina-14*H*. In analogy to the β-alumina-type family the sites are labelled Beevers-Ross (BR) and anti-Beevers-Ross (aBR). Na1 on the BR-site is coordinated by each three oxygen atoms in the layer below and above at distances of 2.828(2) Å plus three oxygen atoms in the same layer at a distance of 3.260(1) Å. A Na atom situated on the idealised aBR-site has each two oxygen atoms above and below at a distance of 2.485(1) Å and three oxygen atoms in the same layer at a distance of 3.261(1) Å. In β-alumina-14*H* Na1 is situated on the BR site and a second, only partially occupied Na2-positionis slightly off the aBR site on a split positions, as indicated by small circles with green filling in Fig. 6(b). In this way the unfavourable position of Na2 between two very close O1-atoms is relaxed by enlarging the Na2-O1-distance from 2.485(1) to 2.600(1) Å. This observed split position of Na2 has previously been described as the so-called mid-oxygen (mO) position.

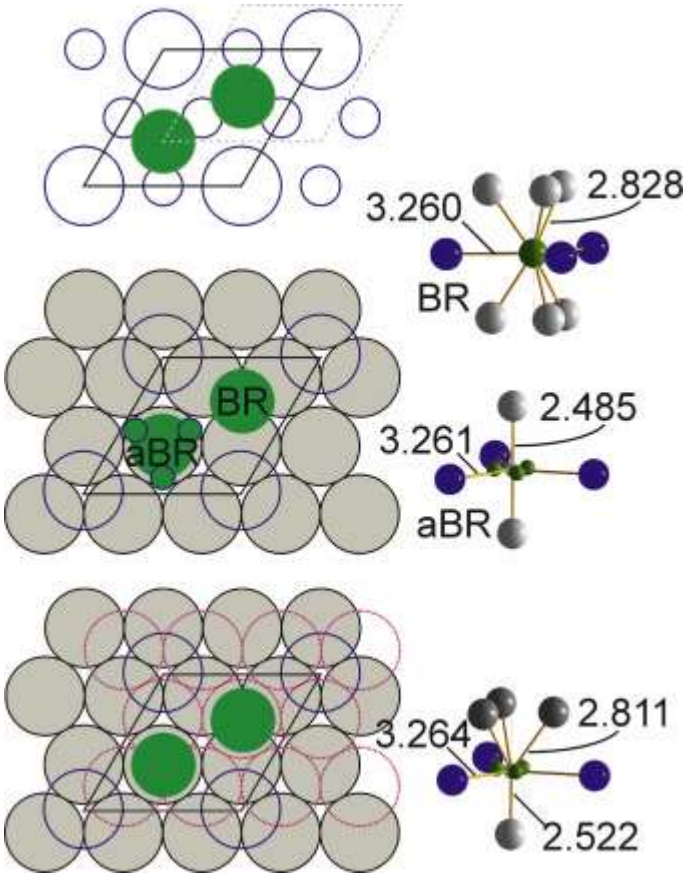

Fig. 6. Ideal geometry of the Na block and coordination of Na. (a) Deficient oxygen layer of the Na-block. Large empty circles with blue rim are O-positions, small empty circles with blue rim correspond to positions that would be occupied by O in a close-packed layer, green filled circles are the two principle positions for Na. Solid outline of the unit cell refers to β-alumina-21*R* &−14*H*, unit cell with broken outline has the origin in the anti-Beevers-Ross site as in β-alumina. (b) The O-deficient Na-containing oxygen layer sandwiched between two adjacent oxygen layers in the same position (circles with grey filling), i.e. in hexagonal close packing (ABA-type stacking) as found in β-alumina-14*H*. (c) In β-alumina-21*R* the deficient oxygen is in a cubic close packed arrangement with adjacent oxygen layers at different positions (ABC-type stacking), one given with grey filling, the other with red dotted line and no filling. See text for further discussion.

Fig. 6(c) shows the oxygen-deficient Na-hosting layer in β-alumina-21*R* in a cubic close packed arrangement with adjacent oxygen layers at different positions ("ABC"-type), one given with grey filling, the other with red dotted line and no filling. The two Na-positions are equivalent and both in seven-fold coordination with either three oxygen atoms above (2.811(1) Å) and one below at a distance of 2.522(1) Å, or the other way round, and three oxygen atoms in the same layer at a distance of 3.264(1) Å. In this cubic close packed environment one Na position corresponds to the two Na-positions BR and aBR in the hexagonal close packed environment. Actually, the positions of Na and O7 in the deficient oxygen layer in β-alumina-21*R* are split around the special positions and not on the three-fold axis, so that the actual Na-O distances (see Table 4) are slightly different from the above values, which were calculated for the case that Na and O7 were situated exactly on the three-fold axis. Another difference between the Na-block in the two structures is the relative orientation of the T6 tetrahedron (see Fig. 7 and Fig. 8): In β-alumina-14*H* they are related by a mirror plane, i.e. the two T6-tetrahedra have the same relative orientation. In β-alumina-21*R* the orientation of the two tetrahedra are related via an inversion centre so that their relative orientation is rotated by 180°.

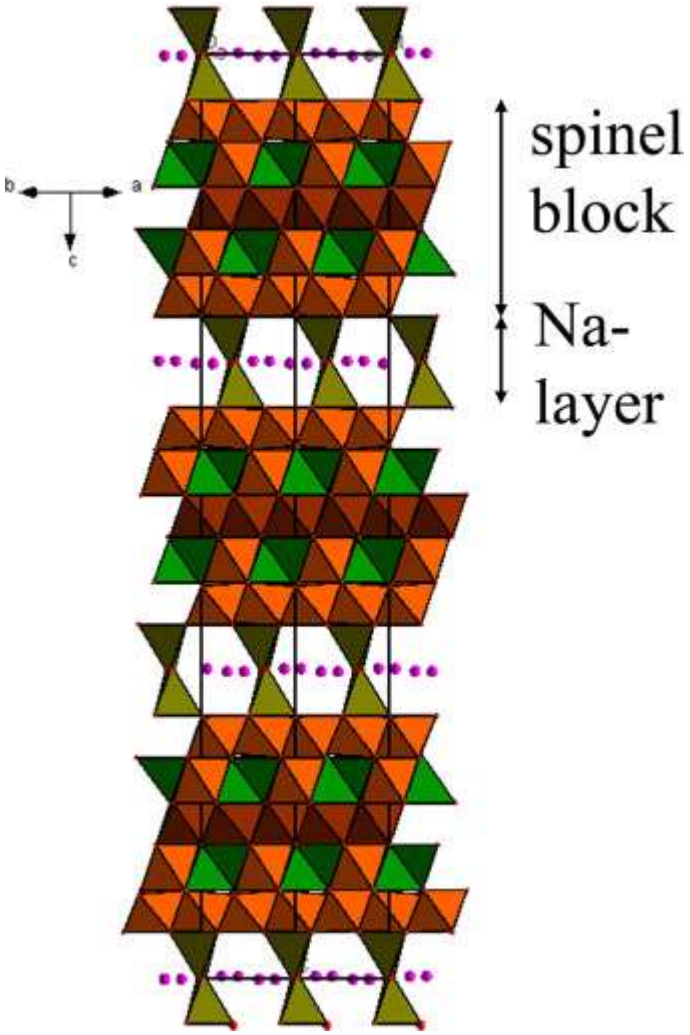

Fig. 7. Projection of the structure of β-alumina-21*R* along [110].

Table 6. Overview and comparison between different polysomes of the β-alumina type families.

	Space-group	**c [Å]**	**Cation layers in Spinel block**	**Number of Spinel blocks per unit cell**	**Sequence of close-packed oxygen layers**	**Stacking sequence of close-packed oxygen layers**	**Suffix [9]**	**Suffix [16]**	**Reference**
β-alumina	P63/mmc **No. 194**	22.60	O-OT-O	2	(ABCA)B **(ACBA)C**	2 × (cccch)	2H(5)	10H	[10]
β”-alumina	R−3m **No. 166**	34.226	O-OT-O	3	(ABCA)B **(CABC)A** **(BCAB)C**	3 × (ccccc)=15 × (c)	3R(5)	15R	[28]
β-alumina-14H	P63/mmc No. 194	32.056(2)	O-OT-O-OT-O	2	(ABCABC)A **(CBACBA)C**	2 × (ccccccch)	2H(7)	14H	This study
β-alumina-21R	R−3m No. 166	48.074(4)	O-OT-O-OT-O	3	(ABCABC)A **(BCABCA)B** **(CABCAB)C**	3 × (ccccccc)= **21 × (c)**	3R(7)	21R	This study

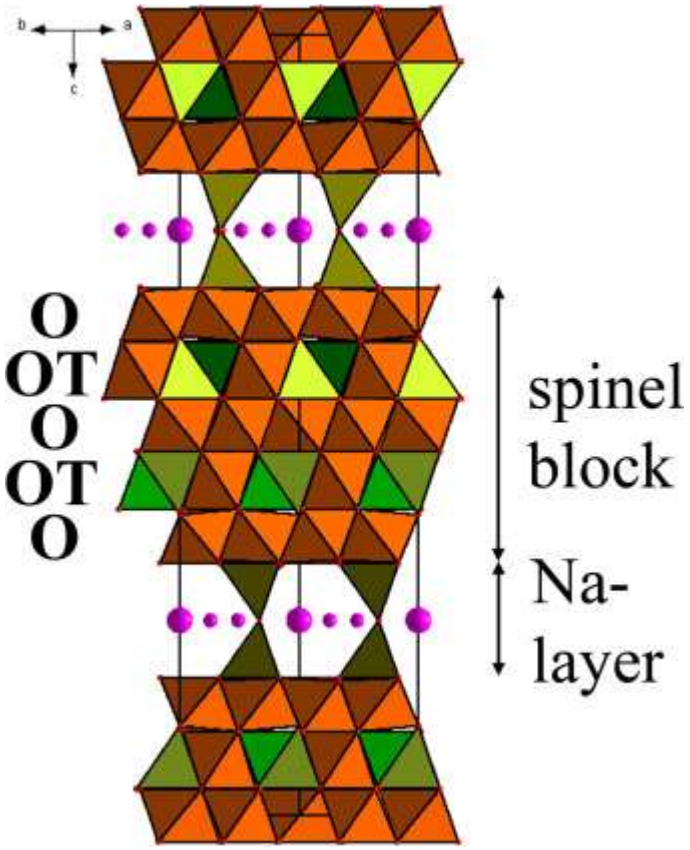

Fig. 8. Projection of the structure of β-alumina-14*H* along [110].

The spinel block is very similar in β-alumina-14*H* and β-alumina −21*R*. A refinement of the Cr-occupancy showed Cr to be present on the octahedral positions M1 and M3 of the **OT**- and the two outer **O**-layers of the spinel block, but not in the central **O**-layer. The octahedra in the two outermost **O**-layers of the spinel-block directly adjacent to the Na-block are rather distorted with M3-O distances ranging from 1.847(2) to 2.037(3) Å and 1.840(2) to 2.043(2) Å in β-alumina-21*R* and β-alumina-14*H*, respectively.

From the larger T-O distances in the tetrahedra T4 and T5 of the spinel block in comparison to the T6-O distances in the Na-block it can be concluded, that Mg is predominantly situated in the spinel-block tetrahedra T4 and T5 whereas in the T6 tetrahedron of the Na- block Al is dominant. Furthermore, the occupation of the spinel-block tetrahedral positions with Mg is supported by a considerably larger bond valence sum for T6 in comparison to T4 and T5 (Table 4 and Table 5).

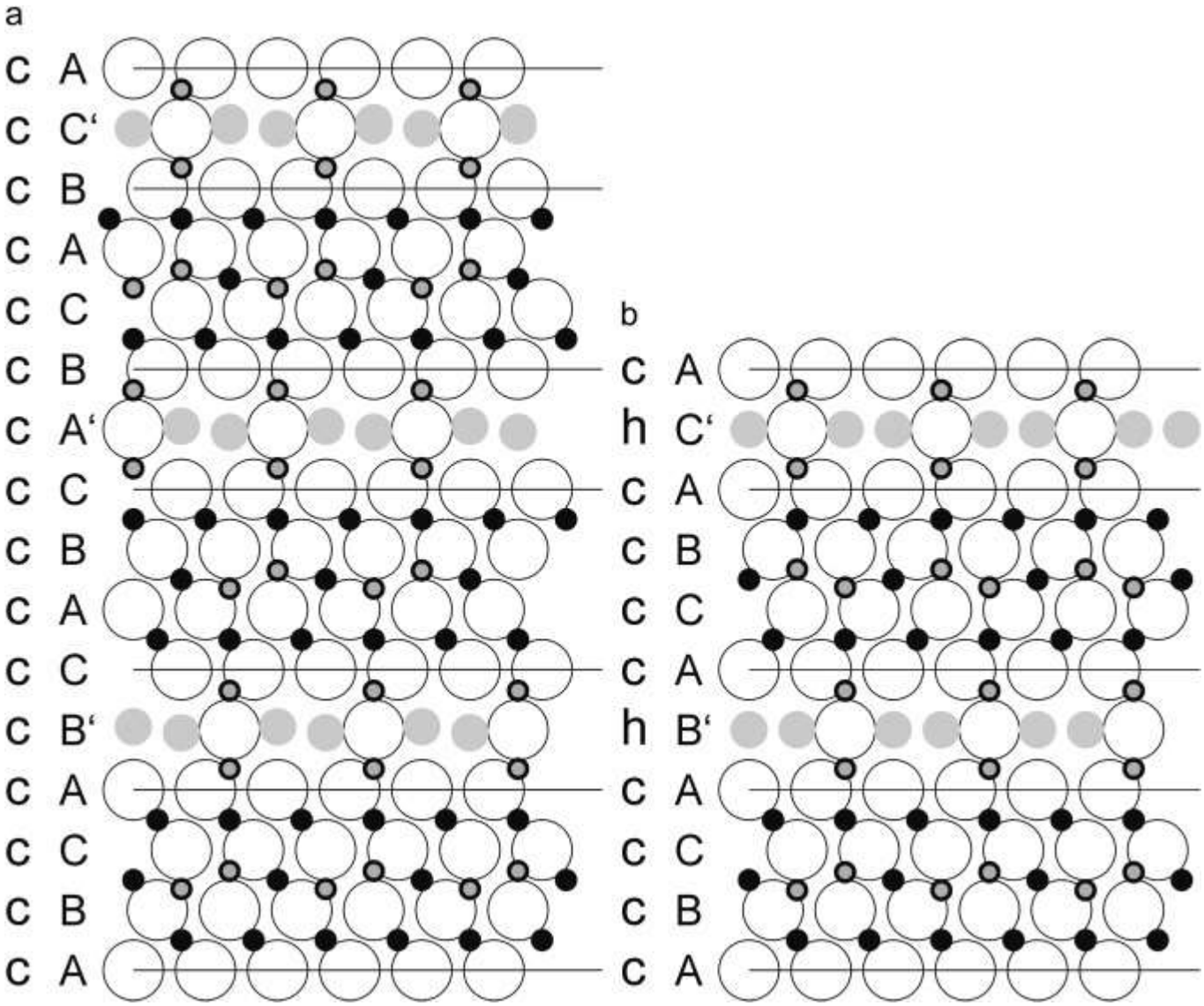

Fig. 9. Stacking of close packed oxygen layers in (a) β”-alumina and (b) β-alumina, symbols as in Fig. 4.

2.3.2. Comparison to β-alumina and β”-alumina

The relationship between β-alumina-21*R* and β-alumin-14*H* is very similar to the relation between β”-alumina [28] and [4], and β-alumina [10] and [22], the two best known members of the β-aluminas. These two structures are likewise composed of a spinel- and a Na-block that is repeated twice in β-alumina and three times in β”-alumina (Fig. 9(a),(b), Table 6). One difference is the size of the spinel block: In β-alumina-21*R* and β-alumin-14*H* the spinel block is composed of six cubic close packed oxygen layers with an **O**-**OT**-**O**-**OT**-**O** arrangement of the cation layers, whereas in β-alumina and β”-alumina the spinel block has only four cubic close packed oxygen layers with an **O**-**OT**-**O** arrangement of the cation layers (Table 6). The composition of the spinel block in β-alumina and β”-alumina is $2\times M_3O_4+ T_2MO_4=T_2M_7O_{12}$. A second difference concerns the Na-block. β-alumina was originally described with one Na atom per formula unit, i.e. one Na atom in the conduction layer of formula NaT_2O_5. With this notation the β-alumina structure type $NaAl_{11}O_{17}$ ($NaT_4M_7O_{17}$) can be explained as an alteration of a Na-block of NaT_2O_5-composition and the above derived spinel block $T_2M_7O_{12}$. However, it was later on realized, that β-alumina often contains an

excess of Na. Especially β”-alumina has been found to contain up to 1.77 Na a.p.f.u (e.g. [21], see also list in [8] and is hence closer to an alteration of a $Na_2T_2O_5$-type Na-block with the spinel block. The additional Na in β”-alumina of traditional $NaAl_{11}O_{17}$ notation is usually charge compensated by Mg^{2+} or other cations of a charge smaller than 3+ that substitute for Al in the spinel block.

In β-alumina-21*R* and β”-alumina all oxygen layers are cubic close packed and the Na-block in β-alumina-21*R* is basically identical to the conduction layer that has been described for β”-alumina (Fig. 6(c)). In contrast to this, β-alumina-14*H* and β-alumina have a mirror plane in the Na-block so that the respective oxygen layer is in a hexagonal close packed environment: For β-alumina the oxygen stacking sequence is 2 × (*cccch*) and for β-alumina-14*H* it is 2 × (*ccccccch*). There has been a long debate about the position of Na in the conduction plane of β-alumina on the possible sites Beevers-Ross (BR), the *anti*-Beevers-Ross (aBR) and the mid-oxygen position (mO). The positions of the BR- and aBR-site are indicated in Fig. 6(b), the mO-site is identical to the position of the small blue circles in Fig. 6(a) and the small green circles with blue rim that indicate the split Na2-position in Fig. 6(b). A reason for the uncertainty of the Na-position is the structural disorder. This is however, together with the invariable non-stoichiometry of all studied β-aluminas, a salient feature of these phases and an important characteristic for their ionic conductivity. The sodium diffusion between the different sites has recently been studied by molecular dynamics simulation [27], which have proven the importance of defect interactions and shown that the Na diffusion is highly correlated.

Applying the same notation as for the two studied compounds, β-alumina could be named β-alumina-10*H* and β”-alumina would correspond to β-alumina-15*R*. A similar nomenclature (see Table 6) has previously been proposed by [9], who had also found additional members of the β-alumina family, e.g. a component with oxygen layers in 3 × (*ccchchchch*) stacking, β-alumina −30*R*(5), or another component with 3 × (*cchch*) stacking, β-alumina −15*R*(5). The additional number in the nomenclature of Bovin and O’Keefe refers to the number of polyhedral layers that repeat as a unit. The stacking sequence and repeat unit as found for β-alumina −21*R* has never been discussed in detail before, although it is very likely identical to the unpublished structure of β””-alumina [9] and [22]. The same stacking as found for β-alumina −14*H* has previously been proposed for β”’-alumina, $NaAl_{15}Mg_2O_{25}$[4], of which a powder diffraction pattern has been recorded and indexed on a hexagonal lattice with *a*=5.62, *c*=31.8 Å. The crystal structures of β-alumina-21*R* and β-alumina-14*H* reported here represent a significant improvement of the previous structure models.

β-alumina-14*H* and β”’-alumina [4] contain Mg and have a relatively large spinel block of five cation layers in contrast to the smaller spinel block composed of only three cation layers found in the Mg-free structure of analogue β-alumina. This might suggest, that Mg stabilises β-alumina polysomes with a larger spinel block. For β”-alumina a certain Mg-content is actually necessary in order to charge compensate for access Na, as β”-alumina generally has a higher Na-content than β-alumina. However, the Mg-content of the two here reported β-alumina polysomes is higher than for any of the previously reported β”-alumina phases. This might be the reason for both β-alumina-14*H* and β-alumina-21*R* to form a spinel block that is composed of five cation layers within six oxygen layers of cubic close packed arrangement, which is different from and larger than the respective spinel block in β- and β”-alumina.

2.3.3. Phase quantification using powder diffraction

The powder diffraction profile of the slag is shown in Fig. 10. Apparent is the presence of severe preferred orientation, which results in enhanced (00l) peak intensities. Especially the (002), (004), and (006) reflections of the 14 *H* polysome are very intense. These peaks also coincide with the (003), (006) and (009) reflections of the 21 *R* polysome. A March-Dollase preferred orientation correction improved correspondence between observed and calculated intensities, but could not completely eliminate this effect. There is also correlation between the phase quantities of the two polysomes, especially if preferred orientation corrections are attempted simultaneously for both polysomes. Therefore, reliable quantification of the different phases in these slags remains a challenge and the phase quantities can only be estimated as 2/3 β-alumina-phases and 1/3 spinel with additional minor chromium and traces of unknown phases in the analysed slag.

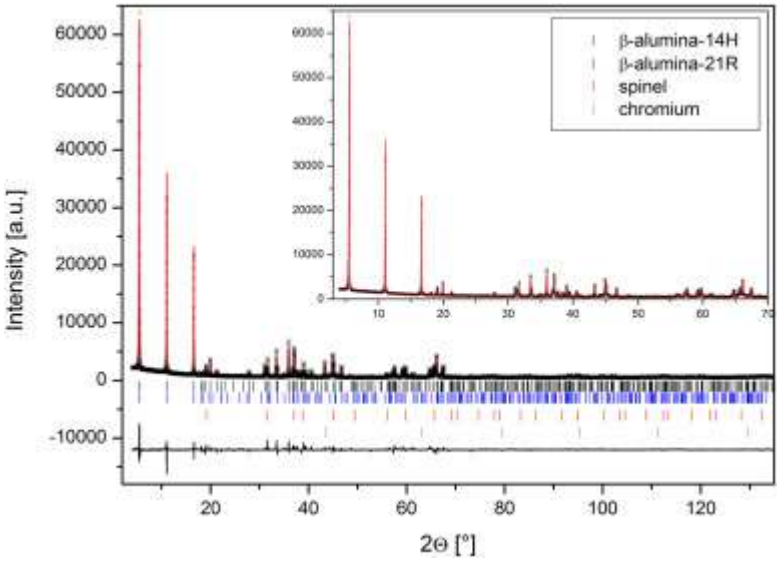

Fig. 10. Result of a Rietveld analysis of a ferrochromium slag. Observed step intensities are given as black crosses, the calculated powder profile is given as red line. Tick marks below the profile show the peak positions of β-alumina-14*H*, β-alumina-21*R*, spinel and chromium (from top to bottom).

References

[1] V. Adelsköld, Ark. Kemi Miner.Geol. 12A (1938) 1–9.

[2] Armbruster Th, Eur. J. Miner. 14 (2002) 389–395.

[3] A. Belsky, M. Hellenbrandt, V.L. Karen, P. Luksch, Acta Crystallogr. B 58 (2002) 364–369.

[4] M. Bettman, L.L. Terner, Inorg. Chem. 10 (1971) 1442–1446.

[5] M. Bettman, C.R. Peters, J. Phys. Chem. 73 (1969) 1774–1780.

[6] C.A. Beevers, M.A.S. Ross, Z. Kristallogr. 97 (1937) 59–66.

[7] P.J. Bhonde, A.M. Ghodgaonkar, R.D. Angal, Proceedings: Infacon XI, New Delhi, India, 2007, pp. 85–89.

[8] D.P. Birnie III, Acta Crystallogr. B 68 (2012) 118–122.

[9] J.O. Bovin, M. O'Keeffe, J. Solid State Chem. 33 (1980) 37–41.

[10] W.L. Bragg, C. Gottfried, J. West, Z. Krist. 77 (1931) 255–274.

[11] I.D. Brown, J. Appl. Crystallogr. 29 (1996) 479–480.

[12] Bruker-AXS, TOPAS Version 4.2: General Profile and Structure Analysis Soft- ware for Powder Diffraction Data, Bruker-AXS, Karlsruhe, Germany, 2009.

[13] R.W. Cheary, A. Coelho, J. Appl. Crystallogr. 25 (1992) 109–121.

[14] M.M. Eissa, K.A. El- Fawakhry, M.L. Mishreky, H.R. EI-Faramawy, Proceedings: Infacon XII, Helsinki, Finland, 2010, pp. 431–438.

[15] J. Faber, T. Fawcett, Acta Crystallogr. B 58 (2002) 325–332.

[16] C. Hejny, Th Armbruster, Amer. Miner. 87 (2002) 277–292.

[17] C. Hejny, E. Gnos, B. Grobety, Th. Armbruster, Eur. J. Miner. 14 (2002) 957–967.[18] K.B. Hueso, M. Armand, T. Rojo, Energy Env. Sci. 6 (2013) 734–749.

[19] S.T. Murphy, C.A. Gilbert, R. Smith, T.E. Mitchell, R.W. Grimes, Philos. Mag. 90 (2010) 1297–1305.

[20] L. Palatinus, G. Chapuis, J. Appl. Crystallogr. 40 (2007) 786–790.

[21] W.H. Pearson, J.F. Lomax, Mater. Res. Soc. Symp. Proc. 293 (1993) 315–321.[22] C.R. Peters, M. Bettman, J.W. Moore, M.D. Glick, Acta Crystallogr. B 24 (1971) 1826 1834.

[23] V. Petříček, M. Dušek, L. Palatinus, Z. Krist. 229 (2014) 345–352.[24] Rigaku, CrysAlis Pro, Yarnton, Oxfordshire, England, 2015.

[25] R. Stevens, J.G.P. Binner, J. Mat. Sci. 19 (1984) 695–715.

[26] D.R. Veblen, Am. Mineral. 76 (1991) 801–826.

[27] B. Wang, A.N. Cormack, Solid State Ion. 263 (2014) 9–14.

[28] G. Yamaguchi, K. Suzuki, Bull. Chem. Soc. Jpn. 41 (1968) 93–99.